



Synthesis of mitochondria-targeted coumarin-3-carboxamide fluorescent derivatives: Inhibiting mitochondrial TrxR2 and cell proliferation on breast cancer cells

Yuanyuan Li, Qun Tang, Yu Xie, Dian He, Kun Yang, Lifang Zheng*

School of Pharmacy, Lanzhou University, Lanzhou 730000, China

ARTICLE INFO

Keywords:

Breast cancer
Mitochondria
Mitochondrial thioredoxin reductase
Coumarin-3-carboxamide
Oxidative stress

ABSTRACT

Targeting specific mitochondrial alterations to kill cancer cells without affecting their normal counterparts emerges as a feasible strategy. Coumarin derivatives have demonstrated the potential anti-breast cancer activities. By coupling coumarin-3-carboxamide derivatives with mitochondria carrier triphenylphosphonium, mitocoumarins **15a-c** were produced and tested as the anti-breast cancer fluorescence agents. Among them, **15b** as the amide-based drug potently suppressed the cell growth in MCF-7, MDA-231, SK-BR-3 breast cancer cells with the IC₅₀ values from 3.0 to 4.1 μM, including the lower cytotoxicity to normal MCF-10A cells with the IC₅₀ value around 45.30 ± 2.45 μM. In mechanistic study for **15b** in MDA-MB-231 cells, it could localize in mitochondria to elicit ROS burst and collapse Δψ_m. Besides, it could deplete GSH by an irreversible alkylation process and moderately inhibit mitochondrial thioredoxin reductase TrxR2, thus leading to aggravate cellular oxidative stress. This study reported **15b** might be useful for the further development into a mitochondria-targeted anti-triple negative breast cancer drug.

Breast cancer (BC) is the most common malignancy which remains a leading killer among women in the world. It is predicted that by 2021, there will be 2.2 million breast cancer cases among women aged 35–49 in China.¹ In breast cancer, mitochondrial alterations have been detected, including increased oxidative stress, aberrant apoptotic machinery, increased membrane potential and deleted or mutated mtDNA.² Targeting these mitochondrial alterations could promote tumor cell death, and decrease drug resistance, possible side effects as well.³ Due to the higher Δψ_m of tumor cells, the triphenylphosphonium cation (TPP) has been discovered as a successful carrier to deliver the drugs to tumor cell mitochondria, leaving the rest of cells unaffected. TPP cation has the delocalized positive charge and hydrophobic surface area, facilitating a fast-mitochondrial matrix uptake independent of the hydrophobicity of cargo molecules.^{4,5} For example, Mito-Tam (**1**),^{6a} Mito-Chlor (**2**)^{6b} and Mito-Vitamin E (**3**)^{6c} have been devised, which are far more efficient in killing BC cells than parental compounds and can bypass multidrug

resistance (Fig. 1A). Encouragingly, Mito-Tam has passed pre-clinical testing and proceeds to phase I clinical trial for Her2^{high} breast cancer.^{6a}

Additionally, overexpression of mitochondrial thioredoxin reductase (TrxR2) is detected in tumors, including BC,⁷ which associates with poor prognosis and therapeutic resistance of cancer.⁸ Inhibition of TrxR2 can increase cellular oxidative stress and activate apoptosis pathway.⁹ The tumor cells are in a higher oxidative stress environment. If a drug could further aggravate oxidative stress and overwhelm the antioxidant defense system, the tumor cells would more easily be killed. Hence, the inhibitors of thioredoxin reductase have been extensively studied. So far, mitocurcumin (**4**)^{10a} and BODIPY-TPA (**5**)^{10b} have been reported to inhibit TrxR2 activity (Fig. 1A).

Natural and synthetic coumarin derivatives are widely used in a number of fields, especially in medicine.^{11,12} Specific to anti-breast cancer activity, coumarin derivatives show sulfatase and aromatase inhibitory activities, including acting as selective estrogen receptor

Abbreviations: ER, estrogen receptor; PR, progesterone receptor; HER2, human epidermal growth factor receptor-2; TPP, triphenylphosphonium; BSO, L-Buthionine-sulfoximine; DCFH-DA, 2',7'-dichlorofluorescein diacetate; FBS, fetal bovine serum; CsA, cyclosporin A; ROS, reactive oxygen species; MTDR, mito-Tracker deep red; TMRE, tetramethylrhodamine ethyl ester; TrxR, thioredoxin reductase; TrxR2, mitochondrial thioredoxin reductase; NMM, N-methylmaleimide; BC, breast cancer; TNBC, triple-negative breast cancer; CCCP, carbonyl cyanide m-chlorophenylhydrazine; TBAB, tetrabutylammonium bromide; HOBT, hydroxybenzotriazole; TFA, trifluoroacetic acid; DMAP, 4-dimethylaminopyridine; EDCI, 1-ethyl-3-(3-dimethyl-aminopropyl)carbodiimide.

* Corresponding author.

E-mail address: zhenglf@lzu.edu.cn (L. Zheng).

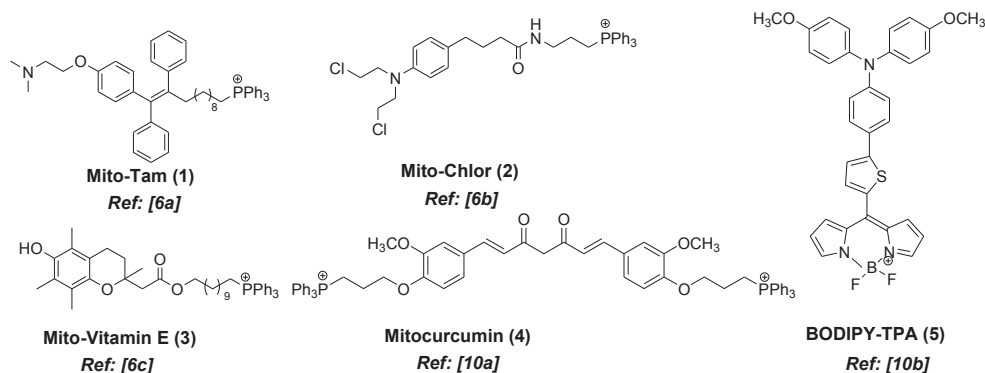
<https://doi.org/10.1016/j.bmcl.2020.127750>

Received 27 October 2020; Received in revised form 27 November 2020; Accepted 9 December 2020

Available online 21 December 2020

0960-894X/© 2020 Elsevier Ltd. All rights reserved.

A The mitochondria-targeted anti-BC drugs (1-3) and TrxR2 inhibitors (4-5)



B The design of Mitocoumarin (15a-c)

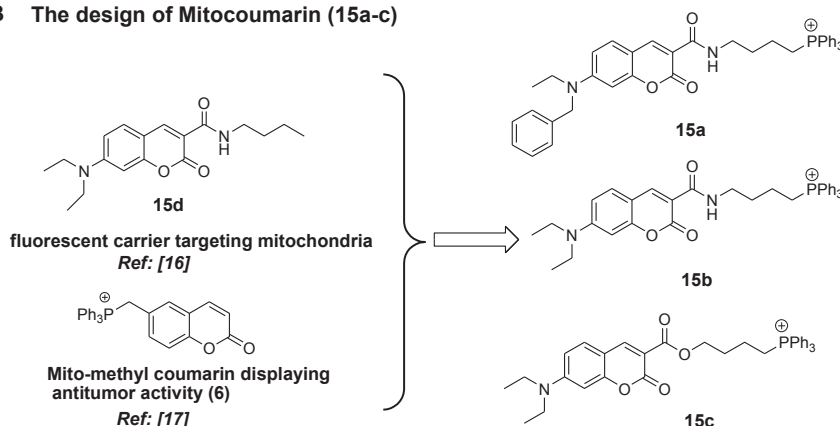


Fig. 1. The overview of introduction.

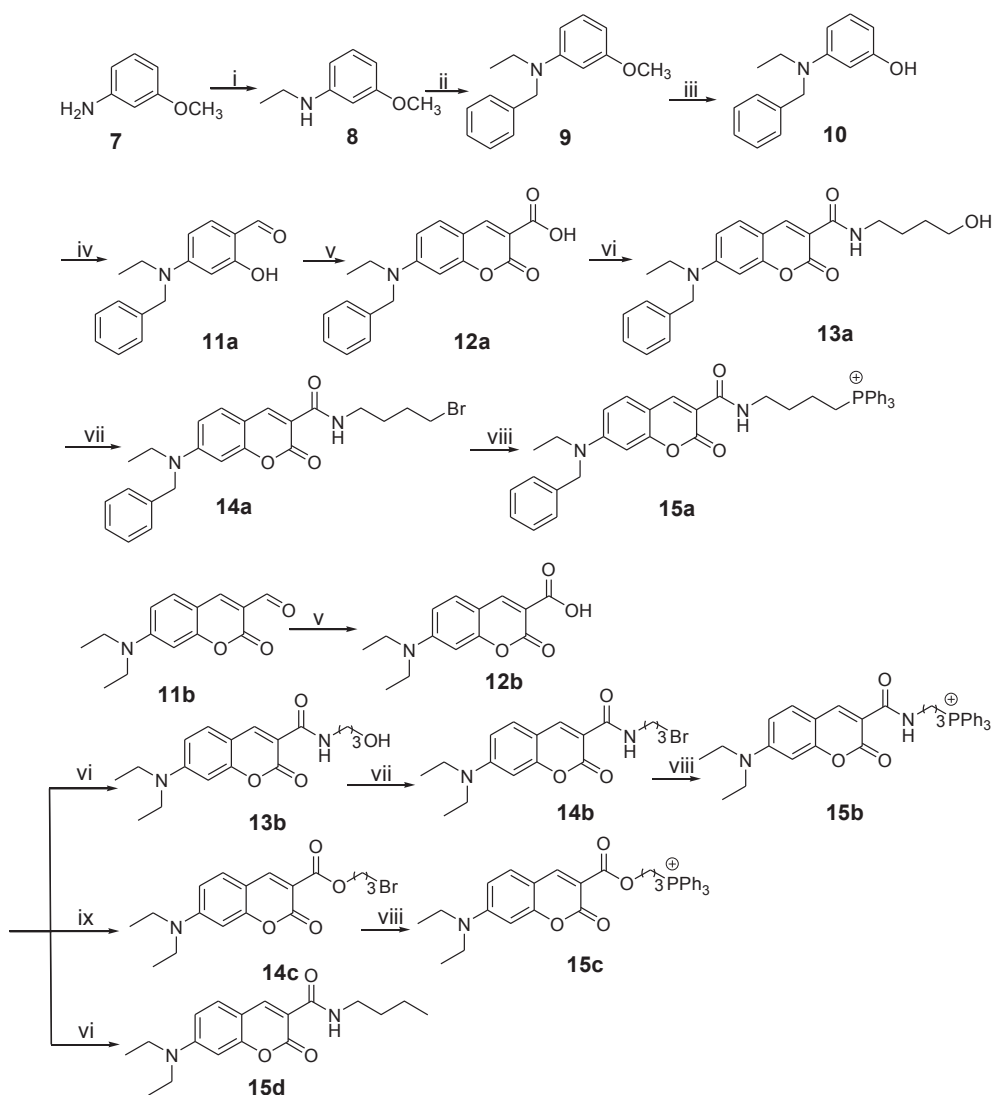
modulators and down regulator.^{13,14} Besides, Xu et al. reported that TPP-coumarin conjugate (**6**) was effective in inhibiting proliferation and inducing apoptosis in HeLa cells.¹⁵ In recent years, the coumarin-3-carboxamide **15d** has been applied as a blue fluorescent vector to deliver drugs specifically to mitochondria in cancer cells together with imaging mitochondria.¹⁶ Therefore, we were motivated to study whether the installment of TPP onto **15d** might produce the novel compound with an optical imaging and cytotoxic activity simultaneously. Therefore, the mitochondria-targeted coumarin derivatives (**15a-c**) were designed and synthesized (Fig. 1B). Next, the physicochemical properties, cytotoxicity toward breast cancer cells (MCF-7, MDA-231, SK-BR-3) were evaluated. The cytotoxic mechanism of the most potent compound **15b** in MDA-MB-231 cells was investigated.

The synthesis of target compounds **15a-c** is depicted in Scheme 1, which are reported herein for the first time and fully characterized by ¹H, ¹³C NMR, and ESI-HRMS (please see the supporting information). Briefly, after the two steps of bromination, compound **9** was obtained from 3-methoxyaniline (**7**), which was treated with BBr₃ to give **10** by demethylation.¹⁷ Subsequently, the alkylated aminophenol **10** was formylated with POCl₃ in DMF to give the corresponding aldehyde **11a** through Vilsmeier Haack conditions. Upon the Knoevenagel condensation, aldehyde **11a** was treated with Meldrum's acid to give the coumarin-3-carboxylic acid (**12a**).¹⁶ After coupling **12a** with amino-butanol and then bromination of the alcoholic function of **13a**, **14a** was obtained.¹⁸ Finally, the reaction of **14a** with PPh₃ in toluene under reflux for 3 days yielded the title compounds **15a**.¹⁹ Besides, compound **15b-d** was synthesized using the similar procedures (Scheme 1). Next, the optical properties and solubility were determined and the results are in Table S1 (please see the supporting information). The compounds **15a-d** displayed the inherent fluorescence with λ_{ex} around 420 nm, and

λ_{em} around 475 nm (Fig. 1A).

We used MTT assay to determine cytotoxicity of **15a-d** on three breast cancer cell lines (MCF-7, MDA-MB-231, SK-BR-3) and one normal breast cell line MCF-10A after 48 h of treatment. It was also determined by Sulforhodamine B method, giving the consistent results as MTT method. Butyltriphenylphosphonium bromide (Butyl-TPP) and **15d** were used as the reference compounds. Drug tamoxifen was a positive control. The results are listed in Table 1. The ranges of IC₅₀ are from 2.73 to 4.90 μM of **15a**, from 3.03 to 3.46 μM of **15b**, from 27.84 to 30.86 μM of **15c**, so the order of cytotoxicity is **15a** **15b** \gg **15c**. The reference compound **15d** and Butyl-TPP did not show cytotoxicity. Compared with tamoxifen, **15a** and **15b** are more potent. It has discovered that cationic compounds can be 100–1000-fold or more concentrated in the mitochondrial matrix, when compared to the extracellular medium.⁴ Based on this principle, we could easily understand why **15b** increased over 30-fold cytotoxicity, compared to the reference compound **15d** (Table 1). Next, the cytotoxicity toward normal cells MCF-10A, the IC₅₀ of **15b** was 3-fold higher than that of **15a**, showing **15b** was less toxic. Finally, the cytotoxicity of **15a-d** against other cancer cell lines were also tested (please see the supporting information, Table S2). The results of this screening suggested that **15a** and **15b** might have a broad spectrum of outstanding anticancer activities. The structure-cytotoxicity relationship for **15a-d** was obtained: (i) installment of TPP carrier dramatically increased the cytotoxicity over 30-fold, confirming that the delivery of drugs to mitochondria was effective and mitochondria was an ideal cellular target for drug distribution; (ii) the changing amide to ester at C-3 significantly weakened cytotoxicity, showing amide was an optimum linker.

The uptake of **15b** and **15c** by MDA-MB-231 cells was measured by flow cytometry.



Scheme 1. Reagents and conditions: i) $\text{CH}_3\text{CH}_2\text{Br}$, K_2CO_3 , NaI , TBAB , CH_3CN , reflux, 8 h, 51.2%; ii) benzyl bromide, K_2CO_3 , DMF , rt, 14 h, 39%; iii) BBr_3 , dichloromethane, 0°C -rt, 1 h, 42%; iv) POCl_3 , DMF , 0°C for 30 min, 60°C for 4 h, 56.9%; v) piperidine, acetic acid, Meldrum's acid, ethanol, rt for 30 min, reflux for 3 h, 69.3%; vi) 4-amino-1-butanol or 1-aminobutane, EDCI , HOBT , dichloromethane, 0°C -rt, 1 h, 55–61.2%; vii) PPh_3 , CBr_4 , acetonitrile, rt, 2 h, 65–74.2%; viii) PPh_3 , toluene, reflux, 72 h, 61–68%; ix) $\text{Br}(\text{CH}_2)_4\text{Br}$, Et_3N , acetone, reflux, 6 h, 61.6%.

Table 1
The cytotoxicity of **15a-d** against breast cancer cells.

Compd.	IC_{50} (μM) ^a			
	MCF-7 ^b	MDA-MB-231 ^b	SK-BR-3 ^b	MCF-10A ^b
15a	4.90 ± 0.34	3.73 ± 0.21	2.73 ± 0.11	15.06 ± 0.52
15b	3.26 ± 0.65	3.03 ± 0.12	3.46 ± 0.09	45.30 ± 2.45
15c	27.84 ± 0.58	29.39 ± 0.23	30.86 ± 0.94	83.66 ± 1.57
15d	>100	>100	>100	>100
Butyl-TPP	57.39 ± 0.63	>100	>100	>100
Tamoxifen	15.21 ± 0.33	35.80 ± 0.15	28.32 ± 31	>50

^a Values represent mean ± SD from at least three independent experiments by MTT assay for 48 h.

Their native blue fluorescence was used to detect data signal. After 2 h of treatment, **15b** and **15c** entered MDA-MB-231 cells in a concentration-dependent manner, as evidenced by the increased fluorescence intensity (Fig. 2A). Besides, incubating with **15b** and **15c** at 8 μM for different duration, the cellular uptake level of **15b** or **15c** increased just within 1.5 h and then decreased over time, giving the highest level at 0.5 h (Fig. 2B). Taken together, the amount of cellular uptake of **15b** was much higher than that of **15c**.

Next, in order to explore why cytotoxicity and cellular uptake level of **15b** were much higher than those of **15c**, we determined the stability.

The stabilities of **15b** and **15c** in methanol–water ($v/v = 1:1$) after three days were measured by HPLC-MS. Chromatogram result showed that **15b** was stable in methanol–water solution, while **15c** produced the degradation reaction, giving three new peaks in the chromatogram (Fig. S1, please see the supporting information). The possible molecular fragments were obtained by analyzing the mass spectrometry data (Table S3, please see the supporting information). Collectively, the intrinsic instability of **15c** impaired cytotoxicity and decreased cellular effective concentration.

Until now, it has been a great challenge in clinical treatment for triple-negative breast cancer (TNBC), which is the most aggressive cancers with a high recurrence rate and rapidly acquired drug resistance among various breast cancer subtypes.²⁰ Therefore, we selected TNBC cells MDA-MB-231 for the following study. Because of higher cytotoxicity and stability of **15b**, we then used laser confocal imaging to explore the subcellular distribution of **15b**. As shown in Fig. 3, blue fluorescence of **15b** and red fluorescence of mitochondrial specific red probe MTR are highly overlapping with the colocalization coefficient value of 0.87, confirming **15b** permeates into mitochondria and localizes in and around mitochondria. Next, we used protonophore CCCP (carbonyl cyanide *m*-chlorophenylhydrazone) to verify whether **15b** entering the mitochondria was $\Delta\psi_m$ -dependent. The protonophore CCCP allows for the dissipation of the proton gradient across the mitochondrial inner membrane, providing a pharmacological method to eliminate $\Delta\psi_m$.²¹ At

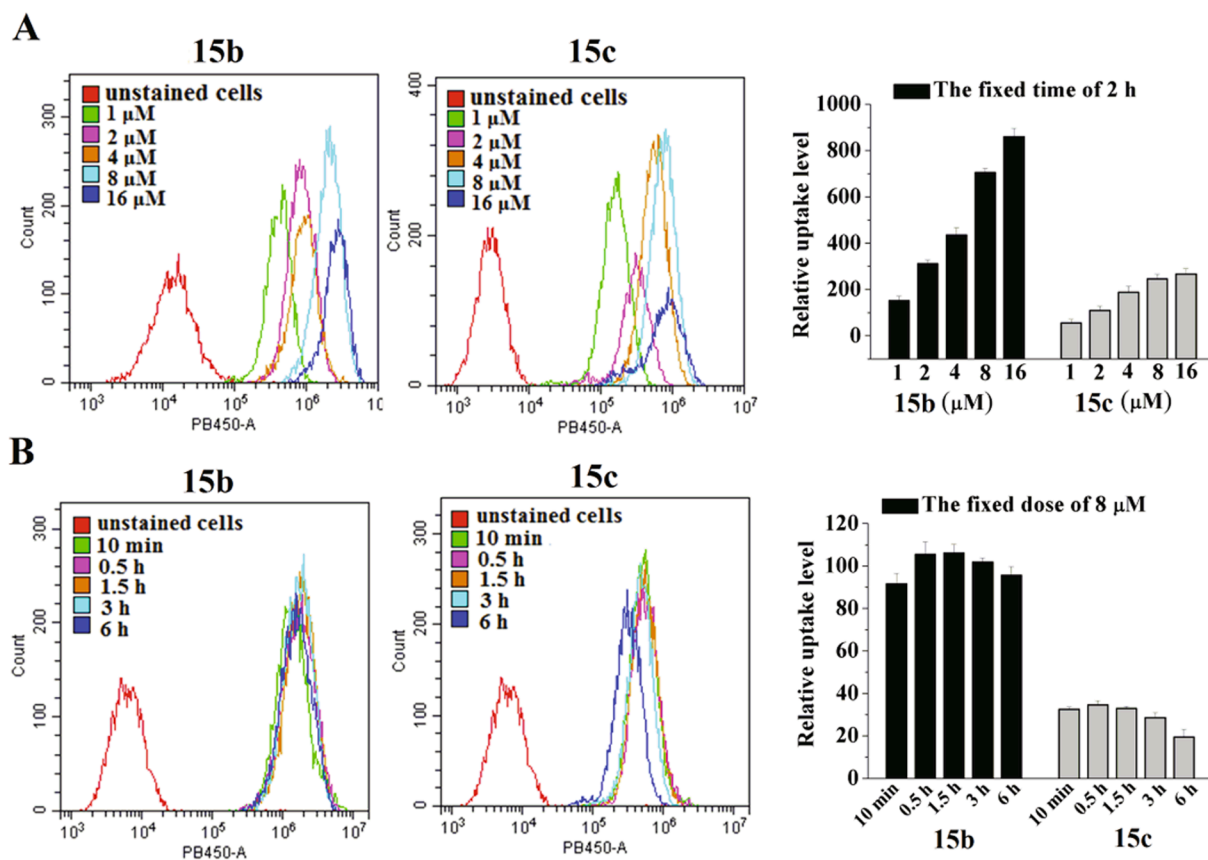


Fig. 2. The relative uptake levels of **15b** and **15c** in MDA-MB-231 cells were determined by flow cytometry. (A) the dose-dependent uptake. (B) the time-dependent uptake. Geometric means of fluorescence intensity values were calculated. Results are presented as means \pm SD, $n = 3$.

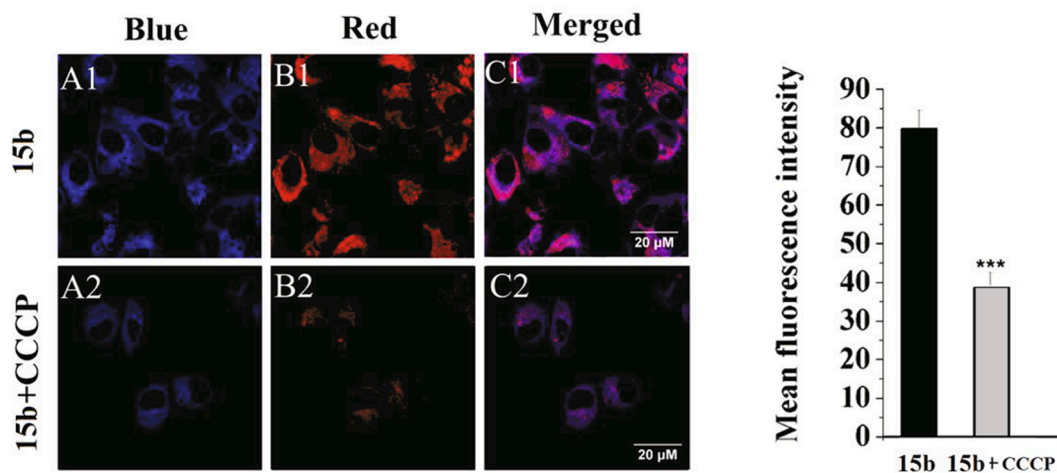


Fig. 3. The visualization of **15b** in mitochondria of MDA-MB-231 cells by laser confocal microscopy. The cells were incubated with $1 \mu\text{M}$ of **15b** for 30 min, and then stained with 100 nm of MTDR (an exclusive red dye for mitochondria) for another 30 min. Besides, the cells were pre-incubated with $20 \mu\text{M}$ of CCCP for 30 min, and then treated with **15b** and MTDR. The blue images are from **15b**, the red images from dye. The mean fluorescence intensity was evaluated by the image J software.

the same voltage on the laser confocal, the images of CCCP pre-treated group showed weaker blue and red fluorescence, showing the mitochondria uptake of **15b** might be reduced to half its amount according to the relative fluorescence intensity (Fig. 3). The results established that **15b** entered mitochondria in a $\Delta\psi_m$ -dependent manner.

The $\Delta\psi_m$ changes in intact cells can imply for mitochondrial functionality during diseases and cell death. Hence, the dissipation of $\Delta\psi_m$ by **15b** was detected by the fluorescent probe tetramethylrhodamine methyl ester (TMRE) which accumulated in the mitochondrial matrix in

proportion to $\Delta\psi_m$.²² The percentages of stained cells decreased dose-dependently, showing the dissipation of $\Delta\psi_m$ (Fig. 4A). The amount of ROS was augmented by **15b** in a dose-dependent manner (Fig. 4B), as evidenced by the increment in fluorescent intensity of DCFH-DA probe. Next, we tested whether mitochondrial permeability transition pore (mPTP) was involved in **15b**-induced cell death. Cyclosporin A (CsA) which is an inhibitor for the formation of mitochondrial permeability transition pore (mPTP) pronounced attenuated cell death at low and medium concentrations, indicating mPTP at least partly involved in

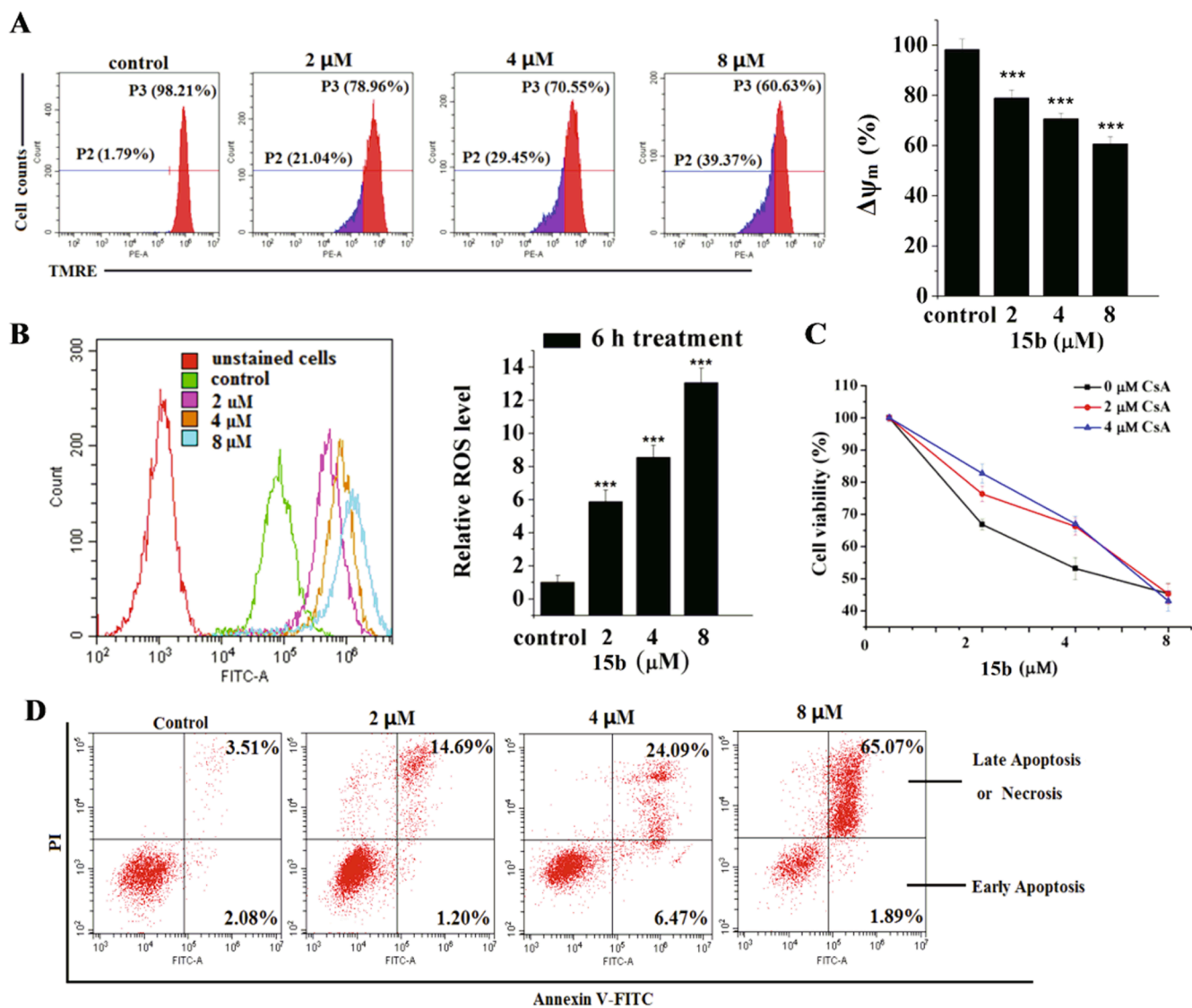


Fig. 4. The effects of **15b** on $\Delta\Psi_m$, ROS level and apoptosis percents in MDA-MB-231 cells. (A) Upon incubation with **15b** for 24 h and then with TMRE probe (100 nM) for 30 min, the $\Delta\Psi_m$ was determined by flow cytometry. (B) Upon incubation for 6 h, then cellular ROS level was probed by DCFH-DA using flow cytometry. Geometric means of fluorescence intensity values were calculated. (C) The cells were pre-incubated with CsA (2 and 4 μM) for 2 h, then exposed to **15b** for 48 h, followed by MTT assay. (D) Upon incubation for 48 h, then apoptosis were detected by Annexin V/PI double-staining assay. Results are presented as means \pm SD, n = 3, ***P < 0.001.

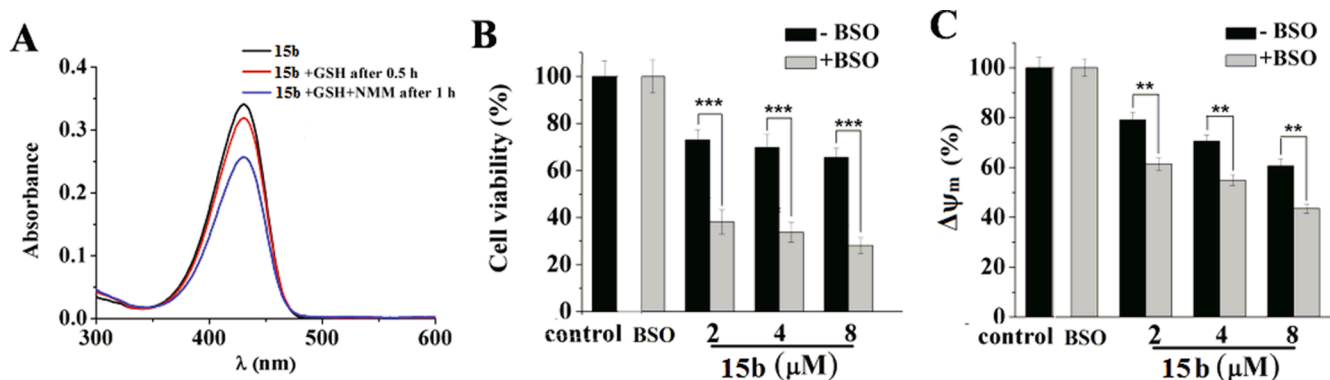


Fig. 5. The chemical interaction of **15b** and GSH and the effects of GSH on **15b**-induced cell death and $\Delta\Psi_m$ collapse. (A) UV-vis absorption spectrum changes for **15b** (10 μM) in the presence of GSH (100 μM) in PBS buffer (pH 7.4) at 37 $^\circ\text{C}$. After the reaction reaches equilibrium, adding *N*-methylmaleimide (NMM, 100 μM). (B) The MDA-MB-231 cells were pre-incubated with BSO (50 μM) for 24 h, then exposed to **15b** for another 24 h, then MTT method was performed. (C) Determination of $\Delta\Psi_m$ using flow cytometry. Results are presented as means \pm SD, n = 3, ***P < 0.001.

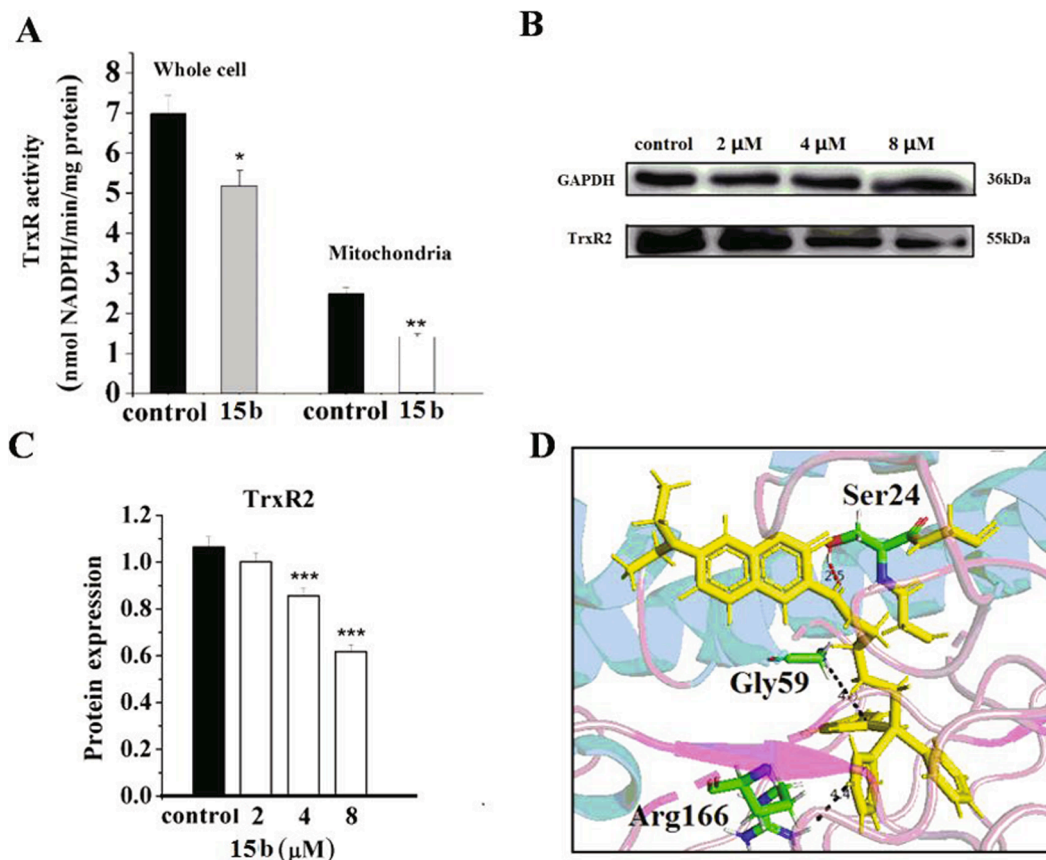


Fig. 6. The effects of **15b** on TrxR activity and protein expression in MDA-MB-231 cells. (A) Upon incubation with **15b** (10 μ M) for 4 h, total cell and mitochondrial extracts were assessed for TrxR activity by Micro Oxidized Thioredoxin Reductase (TrxR) assay Kit. (B) Upon incubation with **15b** (2, 4, 8 μ M) for 48 h, then expression of TrxR2 were determined using Western blot. (C) The level of target protein was calculated by gray scanning. (D) Docking of **15b** in the binding site of TrxR2 in 3D style. For above configuration yellow sticks represent the ligand (**15b**), and red dashed lines represent the hydrogen bonds, black dashed lines represent Pi-interaction. Values are expressed as the means \pm SD; n = 3, * p < 0.05.

the mechanism of cell death²³ (Fig. 4C). Finally, the percentages of apoptotic cells were measured using Annexin V-FITC/PI double staining. The proportion of late apoptotic/necrotic cells increased in response to concentration (Fig. 4D). Consequently, the results indicated that **15b** impaired mitochondrial function and might induce mitochondria-mediated cell death.

Promoting cellular oxidative stress in cancer cells could intensify mitochondrial dysfunction and trigger cell death. Glutathione (GSH) is a key molecular in defending against oxidative stress and removing ROS in vivo.²⁴ Thus, we investigated whether **15b** could deplete GSH amount. The interaction between **15b** and GSH was observed using the UV-visible absorption spectrum. After addition of GSH, the absorption peak of **15b** at 420 nm slightly decreased, indicating the presence of interaction between GSH and **15b** (Fig. 5A). Next, we added *N*-methylmaleimide (NMM) to scavenge all the added GSH but observed that the absorbance still maintained decreasing at 420 nm, proving that the reaction between **15b** and GSH is fully irreversible (Fig. 5A). Further, the effects of GSH on **15b**-induced cell viability and $\Delta\psi_m$ collapse were evaluated by manipulation of cellular GSH level. MDA-MB-231 cells were pretreated with buthionine sulfoximine (BSO) to lower the level of GSH.²⁵ After cells were pretreated with BSO for 24 h, the inhibitory effects of **15b** on cell viability were augmented nearly 50% at each concentration (Fig. 5B). The depolarization of $\Delta\psi_m$ was also increased nearly 13% at each concentration (Fig. 5C). Thus, GSH played a protective role against **15b**-induced cell death and mitochondrial dysfunction and a **15b**-GSH conjugate might be produced.

In addition to decrease cellular GSH level, inhibition of TrxR also can increase ROS concentration and aggravate oxidative stress in vivo.²⁴

Hence, we explored the effects of **15b** on TrxR. Firstly, treatment of MDA-MB-231 cells with **15b** for 4 h decreased TrxR activity in whole cell and mitochondrial extracts (Fig. 6A). Next, the results of western blots showed that **15b** dose-dependently reduced the expression level of TrxR2 (Fig. 6B&C). Thirdly, molecular docking showed that the ligand **15b** had the binding free energy of -49.76 kcal/mol to TrxR2. Ligand **15b** formed the hydrogen bond interactions with Ser24. And the benzene ring formed the Pi-interactions with Arg166 and Gly59 which were conducive to the stable binding of proteins toward small molecules (Fig. 6D). Consequently, the results demonstrated that **15b** could act as a TrxR2 inhibitor and bind with TrxR2 well.

In the present study, we reported on the anti-breast cancer effect and possible mechanism of coumarin-3-carboxamide analogues containing the mitochondria-targeting carrier TPP at C-3 through amide-butyl or ester-butyl chain. Interestingly, **15b** has been found to be a potent anticancer agent against TNBC. **15b** acted by enrichment in mitochondria, alkylation of GSH and inhibition on TrxR2, which could lead to the higher accumulation of ROS and thereby improve oxidative stress in cells. Simultaneously, **15b** also damaged mitochondria function, eventually triggering cell death. Overall, our work showed that delivering drugs to mitochondria and targeting TrxR2 might be a feasible strategy to develop anti-TNBC drugs.

Declaration of Competing Interest

The authors declare that they have no known competing financial interests or personal relationships that could have appeared to influence the work reported in this paper.

Acknowledgements

This work was supported by the Fundamental Research Funds for the Central Universities (Grant No. lzujbky-2018-131), and the National Natural Science Foundation of China (Grant No. 21302079).

Appendix A. Supplementary data

Supplementary data to this article can be found online at <https://doi.org/10.1016/j.bmcl.2020.127750>.

References

- 1 Fan L, Strasser-Weippl K, Li JJ, et al. *Lancet Oncol.* 2014;15:e279–e289.
- 2 Deus CM, Coelho AR, Serafim TL, Oliveira PJ. *Future Med Chem.* 2014;6:1499–1513.
- 3 Neuzil J, Dong LF, Rohlena J, Truksa J, Ralph SJ. *Mitochondrion.* 2013;13:199–208.
- 4 Zielonka J, Joseph J, Sikora A, et al. *Chem Rev.* 2017;117:10043–10120.
- 5 Murphy MP. *Biochim Biophys Acta.* 2008;1777:1028–1031.
- 6 (a) K. Rohlenova, K. Sachaphibulkij, J. Stursa, et al., *Antioxid. Redox Signal.* 26 (2017) 84–103; (b) M. Millard, J.D. Gallagher, B.Z. Olenyuk, N. Neamati, *J. Med. Chem.* 56 (2013) 9170–9179; (c) B. Yan, M. Stantic, R. Zobalova, et al., *BMC Cancer.* 15 (2015) 401.
- 7 Bhatia M, McGrath KL, Trapani GD, et al. *Redox Biol.* 2016;8:68–78.
- 8 Kim MR, Chang HS, Kim BH, et al. *Biochem Biophys Res Commun.* 2003;304:119–124.
- 9 Scalcon V, Bindoli A, Rigobello MP. *Free Radic Biol Med.* 2018;127:62–79.
- 10 (a) S. Jayakumar, R.S. Patwardhan, D. Pal, et al., *Free Radic. Biol. Med.* 113 (2017) 530–538; (b) X. Du, P. Zhang, H. Fu, et al., *Int. J. Pharm.* 555 (2019) 346–355.
- 11 Zhu JJ, Jiang JG. *Mol Nutr Food Res.* 2018, e1701073.
- 12 Emami S, Dadashpour S. *Eur J Med Chem.* 2015;102:611–630.
- 13 Musa MA, Cooperwood JS, Khan MOF. *Curr Med Chem.* 2008;15:2664–2679.
- 14 Dandriyal J, Singla R, Kumar M, Jaitak V. *Eur J Med Chem.* 2016;119:141–168.
- 15 Wang H, Xu W. *Biochem Biophys Res Commun.* 2017;489:1–7.
- 16 (a) K. Yang, Y.Y. Li, Q. Tang, et al., *Eur. J. Med. Chem.* 170 (2019) 45–54; (b) X. Zhang, Q. Ba, Z. Gu, et al., *Chem. Eur. J.* 21 (2015) 17415–17421.
- 17 Sun Q, Tian H, Qu H, et al. *Analyst.* 2015;140:4648–4653.
- 18 Brindisi M, Butini S, Franceschini S, et al. *J Med Chem.* 2014;57:9578–9597.
- 19 Li J, He D, Wang B, et al. *Acta Pharm Sin B.* 2017;7:106–115.
- 20 Hwang SY, Park S, Kwon Y. *Pharmacol Ther.* 2019;199:30–57.
- 21 Caporale T, Ciavardelli D, Ilio CD, Lanuti P, Drago D, Sensi SL. *Exp Neurol.* 2009;218: 228–234.
- 22 Jr RCS, Grotyohann LW. *Biophys J.* 1999;76:469–477.
- 23 Clarke SJ, McStay GP, Halestrap AP. *J Biol Chem.* 2002;277:34793–34799.
- 24 Matsuzawa A. *Arch Biochem Biophys.* 2016;617:101–105.
- 25 Li K, Yang K, Zheng L, et al. *Bioorg Med Chem.* 2018;26:4191–4200.